Alloy Fluctuations Act as Quantum Dot-like Emitters in GaAs-AlGaAs Core–Shell Nanowires

Nari Jeon,[†,#] Bernhard Loitsch,[‡,§,#] Stefanie Morkoetter,[‡] Gerhard Abstreiter,[‡,∥] Jonathan Finley,[‡,§] Hubert J. Krenner,[§,⊥] Gregor Koblmueller,[*,‡,§] and Lincoln J. Lauhon[*,†]

[†]Department of Materials Science and Engineering, Northwestern University, Evanston, Illinois 60208, United States, [‡]Walter Schottky Institut, Physik Department, and Center of Nanotechnology and Nanomaterials, Technische Universität München, 85748 Garching, Germany, [§]Nanosystems Initiative Munich (NIM), Schellingstraße 4, 80799 München, Germany, [∥]Institute for Advanced Study, Technische Universität München, Garching, 85748 Garching, Germany, and [⊥]Lehrstuhl für Experimentalphysik 1, Institut für Physik, Universität Augsburg, 86159 Augsburg, Germany. [#]N.J. and B.L. contributed equally.

ABSTRACT GaAs-Al$_x$Ga$_{1-x}$As (AlGaAs) core–shell nanowires show great promise for nanoscale electronic and optoelectronic devices, but the application of these nonplanar heterostructures in devices requires improved understanding and control of nanoscale alloy composition and interfaces. Multiple researchers have observed sharp emission lines of unknown origin below the AlGaAs band edge in photoluminescence (PL) spectra of core–shell nanowires; point defects, alloy composition fluctuations, and self-assembled quantum dots have been put forward as candidate structures. Here we employ laser-assisted atom probe tomography to reveal structural and compositional features that give rise to the sharp PL emission spectra. Nanoscale ellipsoidal Ga-enriched clusters resulting from random composition fluctuations are identified in the AlGaAs shell, and their compositions, size distributions, and interface characteristics are analyzed. Simulations of exciton transition energies in ellipsoidal quantum dots are used to relate the Ga nanocluster distribution with the distribution of sharp PL emission lines. We conclude that the Ga rich clusters can act as discrete emitters provided that the major diameter is ≥4 nm. Smaller clusters are under-represented in the PL spectrum, and spectral lines of larger clusters are broadened, due to quantum tunneling between clusters.

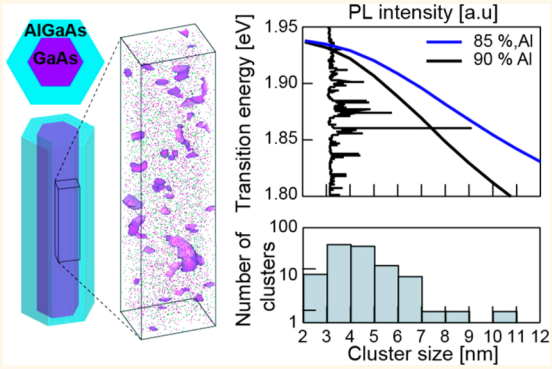

KEYWORDS: nanowire · III–V · heterostructure · atom probe tomography · photoluminescence · quantum dot

GaAs-AlGaAs planar heterostructures are well suited for high-speed electronics and optoelectronics owing to the direct bandgap of GaAs, nearly perfect lattice matching of the GaAs-AlGaAs interface, and a high electron mobility.[1] Since GaAs-AlGaAs heterostructures were realized in nanowire form,[2,3] they have been explored as potential components for ultrasmall, high performance devices including high-electron mobility transistors,[4] lasers,[5,6] and light-emitting diodes.[7,8] This is mainly due to the unique one-dimensional geometry of nanowires, which facilitates formation of radial and axial heterostructures and direct incorporation into Si based devices. Recently, several authors have reported sharp PL emission features, occurring below the band edge of AlGaAs, in GaAs-AlGaAs core–shell nanowires.[9−15] These sharp emission lines imply the presence of a perturbed potential landscape that may localize excitons and degrade carrier mobility. While it is generally desirable to suppress *random* potential fluctuations, well-controlled composition perturbations such as self-assembled quantum dots (QDs) in nanowires[16−18] exhibit unique and potentially useful emission characteristics. In both cases, the correlation of nanoscale composition modulation and optical properties is important fundamental challenge.

Several groups have reported the detection of composition fluctuations in GaAs-AlGaAs core–shell nanowires, by various methods,[9,11] but a statistical correlation between the structure and the optical properties has not been made mostly due to the lack of quantitative information on the composition features.

* Address correspondence to lauhon@northwestern.edu, gregor.koblmueller@wsi.tum.de.

Received for review May 11, 2015 and accepted July 30, 2015.

Published online July 30, 2015
10.1021/acsnano.5b04070

The suggested origins of sharp PL emission features include local alloy fluctuations distributed randomly over the entire bulk-like shell regions[9,11,12] and Ga rich regions acting as QDs confined at the very perimeter of narrow {112}[15] corner facets within the complex hexagonal AlGaAs shell geometry.[10] Rudolph *et al.* attributed contrast undulations in high-resolution transmission electron microscopy (HRTEM) images of nanowire cross sections to alloy fluctuations in the AlGaAs shell, and proposed such features as an origin of the sharp emission lines in PL spectra.[9] However, it was not possible to quantify the magnitude and spatial extent of the alloy fluctuations based on cross-sectional TEM images alone. Around the same time, Heiss *et al.* attributed similar sharp PL features to Ga rich QDs formed at {112} corner facets of the AlGaAs shell based on cross-sectional scanning transmission electron microscopy with energy-dispersive X-ray (EDX) spectroscopy measurement and cathodoluminescence (CL) mapping.[10] The TEM and EDX measurement identified a pyramidal shape cluster of ~10% Al content at the corner facet very close to the nanowire shell surface, and the CL map further revealed a series of bright emitters.[10] However, they were not able to compare the spatial frequency of the pyramidal QDs with that of the bright emitters in the CL map. Moreover, S/TEM analysis of cross-sectioned samples does not resolve all ambiguities regarding the QD structure. Subsequently, Weiss *et al.*[12] recognized similar PL features arising from the AlGaAs shell, and employed surface acoustic wave experiments and simulations to explain their origin. The authors suggested that the QD-like emission centers must be physically separated by at least >10 nm from the next continuum (nanowire surface, core, or radially embedded quantum well) for radiative recombination to become significant. However, the exact sizes, spatial frequencies, and compositional distribution of the proposed alloy fluctuations in the AlGaAs shell were not resolved.

Given the structural complexity of the core–shell nanowires, nanoscale three-dimensional composition information is needed to correlate composition modulations with optical properties. Atom probe tomography (APT) is a technique well-suited to this challenge, as demonstrated in a wide range of nanoscale systems such as QDs and quantum wells.[19–22] Recently, APT analysis of four GaAs-AlGaAs core–shell nanowires identified one Ga cluster that modeling indicated could act as a local emission center.[11] However, the sample volume precluded a statistical correlation of cluster size and spatial distribution with sharp features in PL spectra. Ideally, one would like to be able to determine if the spectral range of the PL features coincides with that of excitonic transitions that the measured alloy fluctuations can generate.

Here we report distributions of the size and composition of Ga rich clusters measured by APT in the AlGaAs shell of GaAs-AlGaAs core–shell nanowires grown by molecular beam epitaxy (MBE).[9] Two complementary methods, isosurfaces and 2D composition maps, are shown to be necessary to identify and characterize possible localized emitters. Variations of the transition energies of the QD-like emitters as a function of their size and composition are calculated by employing single band effective mass modeling including electron–hole interactions.[23] The simulations are used to correlate the size distribution of Ga rich clusters measured by APT with the spectral range of the sharp PL peaks. Furthermore, simulations of quantum tunneling between clusters show how interactions between emitters influence the photoluminescence characteristics, and explain why not all Ga clusters produce photoluminescence peaks. This framework of correlated tomography, optical analysis, and modeling can also be applied to other complex heterostructures of mixed dimensionalities with useful optical properties.[16–18]

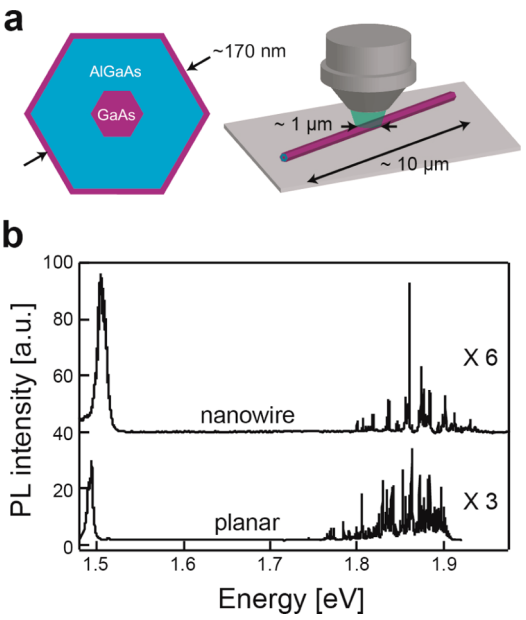

Figure 1. (a) Schematics of core–shell nanowire and PL measurement. (b) PL spectra from a core–shell nanowire with a 60 nm thick shell and reference planar sample of comparable composition. The higher energy portions of the PL emission spectra (>1.6 eV) are multiplied by the indicated factors, and the nanowire emission is offset for visibility.

RESULTS AND DISCUSSION

Micro-PL spectra were acquired from isolated GaAs-AlGaAs core–shell nanowires, consisting of a ~40–50 nm diameter core and a 60 nm-thick AlGaAs shell (nominal Al mole fraction 30%) capped with 5 nm of GaAs (Figure 1a). The PL spectrum in Figure 1b, recorded at 10 K using a continuous-wave laser diode emitting at 532 nm for excitation (spot size of ~1 μm), displays a series of sharp emission lines in the range of 1.80–1.94 eV. These emission lines lie above the emission associated with GaAs interband transitions at 1.52 eV and below the band

edge of AlGaAs (*i.e.*, 1.95 eV for an Al-content of x(Al) = 0.30). Hence, we attribute the PL emission to the AlGaAs shell region. When the peaks are fitted by Lorentzian line shapes, the line widths of most sharp peaks range from ~100 to ~500 μeV (spectral resolution: 80 μeV) and some of the sharp peaks are overlapped with envelope peaks (see Supporting Information and Figure S1 for details). Peaks with wider line widths are likely superpositions of multiple peaks. The spectral resolution is not sufficient to distinguish between recombination from ground states and excited states. A PL spectrum from a reference planar sample grown on equivalent (110) plane and under identical conditions also shows similar sharp emission lines in the range of 1.75−1.90 eV with similar line widths of ~100 to ~400 μeV (lower panel of Figure 1b). Thus, both the nanowire and planar sample exhibit nearly identical spectral characteristics. We note that there is a large body of literature describing sharp PL emission features in GaAs-AlGaAs heterostructures, most of which concerns emission from GaAs quantum wells (QWs) or QDs in AlGaAs barrier layers. In contrast, we are here concerned with emission from the AlGaAs itself, while noting that composition fluctuations that occur in high Al-content AlGaAs thin films and heterostructures[24−28] also influence emission from adjacent GaAs nanostructures.[14,24] In order to correlate PL spectra with their underlying structural origins, it is necessary to establish the magnitude and extent of AlGaAs composition fluctuations and analyze the degree of confinement they would produce.

APT analysis was performed by LEAP 4000X Si under laser conditions of 0.1−1 pJ pulse energy and 250 kHz pulse rate at the base temperature of 23 K and a target detection rate of 0.2% (see also Supporting Information for further details and mass spectra). A detailed analysis of the core−shell nanowire shows that the composition fluctuations in the AlGaAs shell exceed those of a random alloy (Figure 2), as might be expected on the basis of past analysis of GaAs-AlGaAs (Al mole fraction: 30−38%) heterostructures.[25−27] Two rectangular regions of interest (ROIs) were selected (left: $14 \times 7 \times 470$ nm^3, right: $20 \times 15 \times 470$ nm^3) from the AlGaAs shell reconstruction to quantitatively test the degree of randomness and examine the nature of Ga rich regions (Figure 2(a)). Al rich bands extend along ⟨112⟩ directions (Figure 2(b)), as has been reported previously.[9,11,29] Here, the two ROIs selected for analysis of composition fluctuations exclude the Al rich bands, as these regions do not show Ga clusters localized within the bands. Deviations from random alloy fluctuations were identified by frequency distribution analysis (FDA), in which the APT data is divided up into 3D volume elements (voxels) containing a given number of atoms. The mole fraction of a specific element in each voxel is calculated and the distribution of the number of voxels of a given composition is then compared to the pseudobinomial distribution expected for a random ternary III−As alloy. The voxels

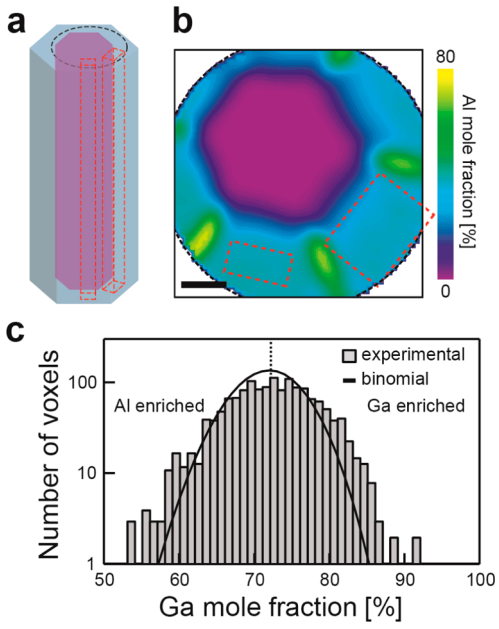

Figure 2. (a) 3D schematic of GaAs core AlGaAs shell nanowire (GaAs capping layer not depicted). The oval indicates an approximate location of the field of view of APT (b). The left and right red boxes show approximate locations of the ROIs used for identifying Ga rich clusters. (b) Detector (top) view of 2D Al mole fraction map in region shown by black circle in (a) (scale bar: 10 nm). (c) Frequency distribution of Ga composition from the left ROI ($14 \times 7 \times 470$ nm^3) at a voxel size of 100 atoms. The solid black line gives the pseudobinomial distribution expected for a random alloy.

used here contain 100 atoms, which is approximately a $2.4 \times 2.4 \times 2.4$ nm^3 cube. Qualitatively, the experimental frequency distribution curve is flattened and is broader than the binomial distribution, suggesting the presence of Ga rich clusters. Quantitatively, the FDA with a χ^2-test indicates that the alloy distribution deviates from that of a random alloy with 99.99% confidence level $p < 0.0001$ (Figure 2(c)). For example, 15 voxels (~1% of the observed distribution) have a Ga mole fraction equal to or higher than 85%, while the random distribution predicts that only ~2 voxels (~0.08% of the binomial distribution) should have a Ga mole fraction ≥85%. The corresponding results for the planar sample are similar (Supporting Information S6). In both cases, growth occurs on the nonpolar (110) planes, *i.e.*, planar growth on the (110) GaAs substrate surface and nanowire growth on (110) sidewall facets. From a surface and crystallographic point of view, the surface chemistry and growth mechanisms are expected to be identical. Since identical growth fluxes and temperatures were used, similar structural features are found in both cases. The FDA provides a useful statistical picture of the alloy averaged over the entire data set. For a direct correlation between PL spectra and composition fluctuations, the location, composition, and size of individual features need to be analyzed.

Ga rich clusters were identified with isosurfaces of constant composition, and their size distribution was

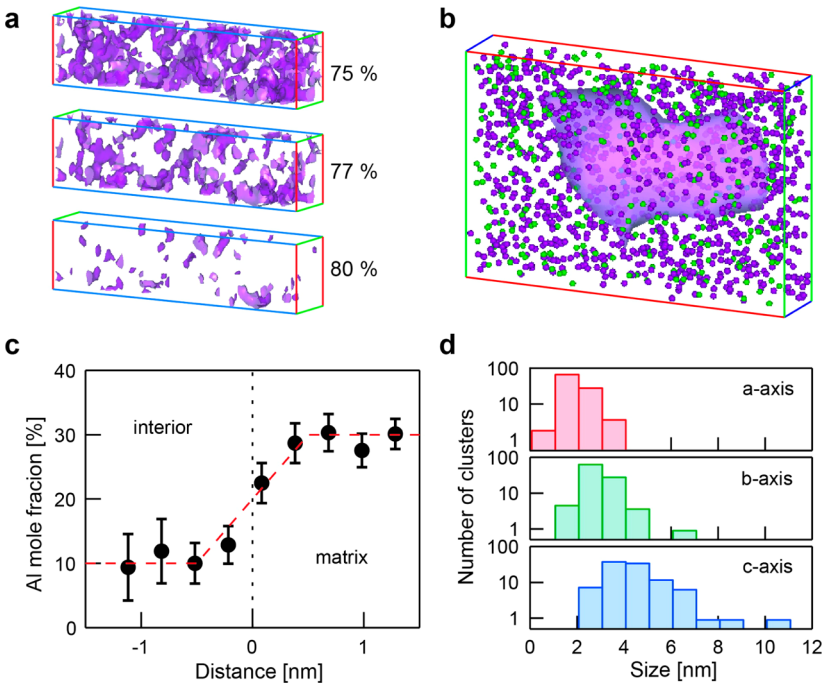

Figure 3. (a) Isosurfaces with increasing threshold Ga mole fractions (ROI: 20 × 15 × 80 nm^3). (b) 3D atom map of including Ga rich region with a translucent isosurface of 80% Ga mole fraction (ROI: 9 × 5.7 × 2.7 nm^3). Purple and green dots represent Ga and Al atoms, respectively. (c) Proxigram generated on the basis of the isosurface shown in (b). The red dashed line represents a linear Al mole fraction profile from 10 to 30% over a 1 nm interface region. (d) Distributions of three axes (*a*-axis, *b*-axis, and *c*-axis) of the Ga rich clusters when they are approximated as triaxial ellipsoids.

analyzed (Figure 3). We note that morphology of isosurfaces changes from an open connected surface to a closed surface as the threshold Ga mole fraction is increased from 75 to 80% (Figure 3(a)). Closed isosurfaces were identified at the interface between Ga rich regions and the matrix by examining isosurfaces of 75−80% Ga mole fraction and proxigrams based on three criteria: (1) a proxigram of a cluster displays a constant or increasing trend of Ga mole fraction toward a center of the cluster; (2) a cluster surface is the largest enclosed surface among the surfaces satisfying the condition (1); and (3) a cluster does not comprise smaller clusters. Figure 3(b) identifies a representative Ga-rich region defined by a closed 79% Ga mole fraction isosurface. The Ga-rich region is 6.9 × 4.8 × 2.8 nm^3 when it is treated as a triaxial ellipsoid. The boundaries of this cluster were analyzed by a proximity histogram, or proxigram, which is a composition profile along the path of steepest descent. The proxigram of the isosurface in Figure 3(b) shows that the Al composition changes from ∼10 to ∼30% within a distance of ∼1 nm (Figure 3(c)).

To facilitate statistical analysis of many clusters, the size distribution of similar Ga rich regions was characterized by approximating individual clusters as triaxial ellipsoids (Figure 3(d), Supporting Information Figures S4, S5). As discussed below, this choice is motivated by the finding that at least one dimension of the cluster must be larger than ∼4 nm to produce the observed discrete emission features. The major axes of ∼91% of the Ga clusters identified by isosurfaces lie in the range of 2−5 nm, and there is no discernible orientation with respect to the nanowire axis. Two Ga rich regions of 8 nm or larger were found by isosurfaces in the two ROIs. However, there are also medium size Ga rich regions within open 75−80% Ga isosurfaces that could still act as localized emitters. We therefore examined a series of 2D composition maps generated from 1 nm thick slices along *z*-axis of the large ROI (20 × 15 × 470 nm^3) (Figure 4(a)) to identify additional candidate localized emitters. A representative 2D composition map shows that the largest extent of the Ga enrichment is ∼6.4 nm (Figure 4(b)) for this cluster. The boundary composition profile was measured with a proxigram starting from an isosurface of 84% Ga mole fraction (Figure 4(c)). The interface width is larger than that of the example in Figure 3(b) above, but the dimensions of the feature are similar. There also exist Al enriched regions, which appear as green regions in Figure 4(a) and (b). Overall, by systematically examining isosurfaces and 2D composition maps, the densities of small (2−5 nm) and medium (5−8 nm) clusters was determined to be 77 and 48 μm^{-3} respectively, and two large (8−11 nm) size clusters were found. In the simulations below, these dimensions refer to the largest axis.

The compositional analysis above enables determination of the confinement potentials experienced by excitons that produce QD-like emission. Transition energies of excitons in these potentials were calculated

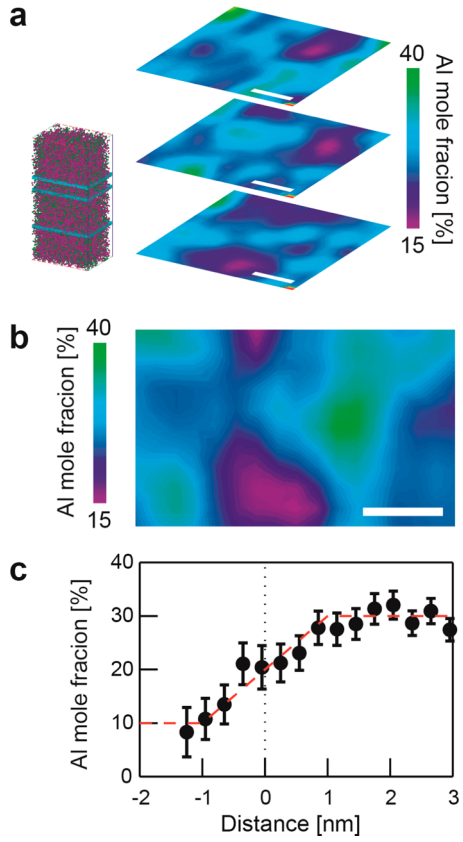

Figure 4. (a) Examples of 2D composition maps containing Ga rich regions. The inset shows the regions (20 × 15 × 1 nm^3) from which the 2D composition maps were extracted (scale bars: 5 nm). (b) 2D composition map of Ga rich region with ~6.4 nm size. (scale bar: 5 nm) (c) Proxigram of the Ga rich region in (b) generated from an isosurface of 84% Ga mole fraction. The red dashed line represents a linear Al composition profile from 10 to 30% over a 2 nm interface region.

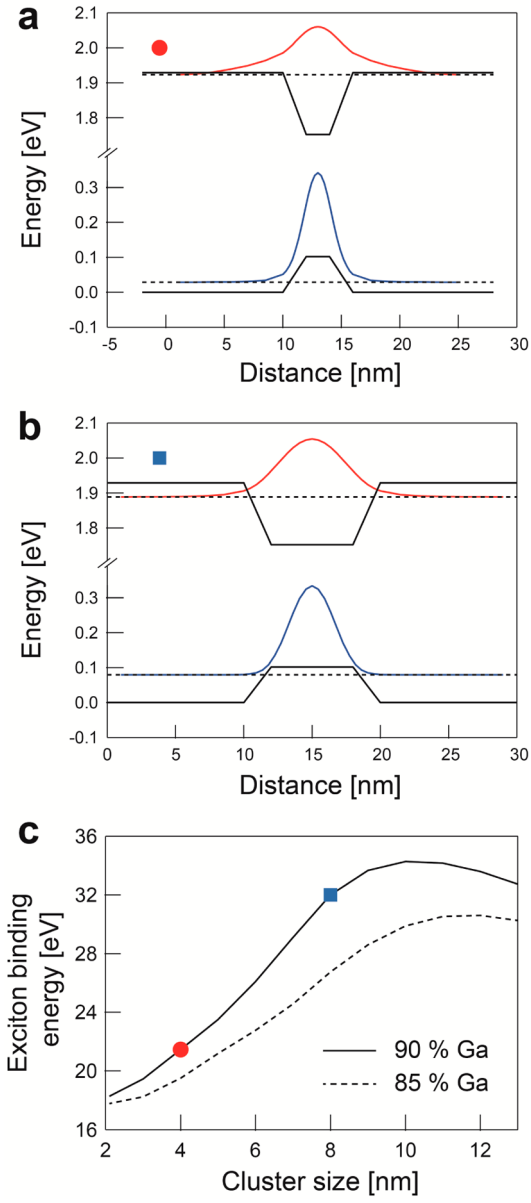

Figure 5. Electron (red) and hole (blue) wave functions of (a) 4 nm and (b) 8 nm QD with a Ga content of 90% and a 2 nm wide interface. The band profile of the confinement potential (black solid lines) and the energetic positions of the electron and hole states (black dashed lines) are also depicted. (c) Exciton binding energy as a function of QD size. Red circle and blue square represent binding energies for the QDs shown in (a) and (b), respectively.

using nextnano^3 including electron−hole interactions. The simulated clusters were encircled by either a 1 or 2 nm wide interface region consisting of a linear gradient in the Ga molar fraction to match the APT analysis. Furthermore, the clusters are assumed to be ellipsoidal to illustrate trends in PL with size; Figure S5 in the Supporting Information indicates that a triaxial ellipsoid with axis ratios of 1:1.5:2.3 represents a typical cluster in the distribution. Figure 5(a) and (b) shows simulations of electron and hole wave functions for cluster sizes of 4 and 8 nm to illustrate the improved confinement of the wave function for the larger clusters. Notably, the spatial extent of the wave functions for the 4 nm cluster suggests that tunneling between closely spaced clusters is likely. The effect of the larger spatial extent of the wave function for smaller clusters, *i.e.*, weaker localization, can also be seen in the simulated excitonic binding energy depicted in Figure 5(c) for two different Ga mole fractions (85 and 90%) in the cluster. As the QD size decreases below ~10 nm the weaker localization decreases the overlap of electron and hole wave functions, hence decreasing the excitonic binding energy. Details about how excitonic effects are included in the nextnano^3 simulation are described in the Methods section.

To correlate the size distribution of the Ga rich clusters and the spectral range of the sharp PL emission lines, transition energies were calculated as a function of QD size at different Ga mole fractions (85 and 90%) and interface widths (1 and 2 nm) (Figure 6(a)). One can see that the potential minimum (arising from Ga mole fraction) has a stronger influence on confinement than the interface width. For example, the experimentally

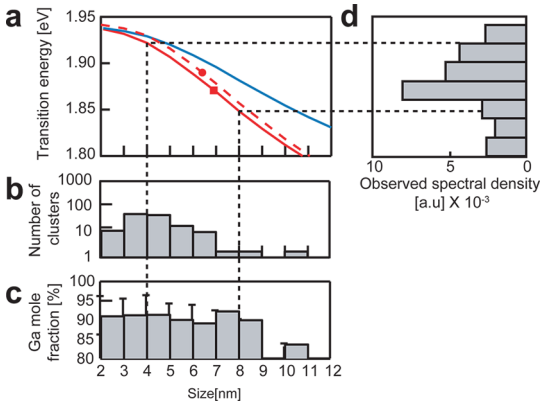

Figure 6. (a) Simulated transition energies for Ga rich clusters as a function of cluster size for two different Ga mole fractions (red: 90%; blue: 85%) and interface widths (solid lines: 1 nm; dashed line: 2 nm). The circle and square represent the transition energies for the clusters shown in Figure 4(b) and Figure 3(b), respectively. (b) Size distribution of the *c*-axis of the triaxial ellipsoids for the Ga rich regions detected with isosurfaces. (c) Distribution of Ga compositions for different sizes of clusters. (d) Spectral density represented as a histogram of PL counts by energy in 0.02 eV bins. Transitions from 4 to 8 nm clusters are most abundant. Dashed lines are guides to the eye.

identified clusters shown in Figures 3(b) and 4(b) both correspond to transition energies of around 1.88 eV (marked as filled circle and filled square in Figure 6(a)). For a broader comparison, Figure 6(b) and (c) show the measured size distribution of clusters and the average Ga mole fraction at different cluster sizes, respectively. The average maximum Ga mole fraction is $\sim 90 \pm \sim 5\%$ for 2−7 nm diameter clusters measured with isosurfaces (Figure 6(c)). We therefore conclude that clusters of 4−8 nm produce the high density of PL peaks seen between ~1.85 and ~1.92 eV in Figure 1(b), while noting that some peaks in Figure 1(b) are likely superpositions of multiple peaks, as described in the Supporting Information. There are fewer clusters within the excitation volume in the 8−11 nm size range, and they produce the lower density of PL peaks at lower energies. However, a comparison of the spectral density above ~1.90 eV (Figure 5(d)) with the cluster density (Figure 5(a)) shows that the numerous clusters with major diameter <4 nm do not make a representative contribution to the PL emission, which should be greater than 1.90 eV. Weiss *et al.* previously considered the influence of tunneling on the PL spectra of core−shell nanowires, finding that tunneling from QD-like centers with low emission energy (<1.7 eV) into the GaAs core and/or cap layer competes with radiative recombination at distances of ~10 nm.[12] For the small clusters, this effect should also be present. Moreover, for small clusters, the wave function is sufficiently delocalized to enable additional tunneling between clusters, as shown below. This effect is expected to enhance the nonradiative loss channel identified by Weiss *et al.* and lead to efficient depopulation of small clusters.

A more quantitative correlation of cluster density and PL features should take into account the possibility that excitons can tunnel between clusters. In particular, rapid transfer of excitons from small to larger clusters could account for the strongly decreasing emission above 1.90 eV (Figure 1(b), Figure 5(a) histogram). Furthermore, intercluster coherent quantum mechanical coupling[30−32] and phonon-mediated interactions[33] have been demonstrated in planar QD architectures. We therefore extended the simulations to account for single particle tunneling between a typical cluster of diameter $d_1 = 6$ nm (corresponding to the peak in the size distribution) and a cluster of diameter d_2, which is varied from 3 nm (asymmetric double-cluster) to 6 nm (symmetric double-cluster). Because intercluster coupling increases dramatically with decreasing intercluster spacing s_c,[30] we varied s_c (defined as the center−center separation) from highly separated ($s_c > 30$ nm) to closely spaced ($s_c < 10$ nm). Note that for this definition, the effective barrier between the two clusters is 1 nm for the smallest s_c. Additional details of the calculations, and plots of coupled cluster wave functions, can be found in the Supporting Information.

Figure 7 summarizes the key result that for the experimentally observed intercluster separations and cluster sizes, energy renormalizations ΔE in the meV-scale are expected; the majority of clusters are neither isolated nor noninteracting. Since localization in larger clusters is energetically preferred, tunneling influences which clusters are emitting and the line widths of those that do. A statistical analysis of s_c from the APT data (Figure 7(b)) shows intercluster separations extending from a few to greater than 10 nm, with a mean value 7 nm. Hence, we expect sizable of downshifts $|\Delta E| >$ 1 meV for the ground state in the abundant double cluster configurations, and hence a broadening of the PL peaks compared to those of isolated clusters. For context, the calculated typical $\Delta E > 2$ meV for the ground state exceeds observed PL line widths by a factor of 5 to 10, and matches typical energy shifts between different occupancy states (biexciton, charged excitons) in this system.[12] We caution that the possibility of tunneling between clusters and from clusters to the GaAs core recommends against a direct correlation between the number of peaks in a given energy window and the number of clusters of a particular size. The tunneling can explain, however, the strong attenuation of emission above 1.90 eV. We note that direct and tangible proof of coherent intercluster coupling could be attained in future experiments employing electric[31,32] and magnetic fields.[34]

Finally, we note that our simulations only account for coherent quantum mechanical tunneling coupling. In addition, phonon-enhanced carrier transfer has been found to occur in weakly coupled QD structures on picosecond time scales even in the case of large detunings.[33] Such processes are also expected in our

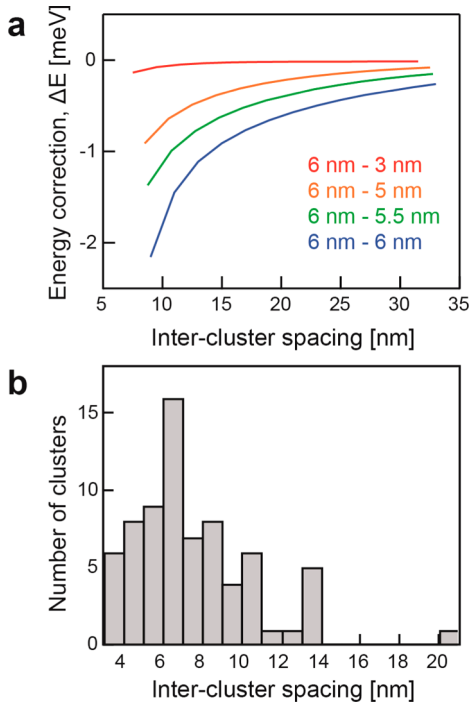

Figure 7. (a) Shift in energy of the ground state of different cluster combinations with respect to the single cluster energies. The legend indicates the size of each cluster in the simulated pair. (b) Histogram of intercluster center-to-center spacings.

systems and lead to an efficient channel for carrier redistribution within the nanowire shell. Taken together, our simulations unambiguously show that for nanowires with moderate cluster densities, the simple picture of isolated and noninteracting clusters cannot provide an adequate description of the dominant photoluminescence characteristics.

CONCLUSION

APT was used to reveal structural and compositional features that give rise to sharp PL emission spectra in GaAs-AlGaAs core−shell nanowires. Nanoscale ellipsoidal Ga-enriched regions were identified in the AlGaAs shell, and their compositions, size distributions, and interface characteristics were analyzed. Simulations of exciton transition energies in ellipsoidal QD-like emission centers were used to relate the Ga nanocluster distribution with the distribution of sharp PL emission lines. We conclude that the Ga rich regions above a threshold diameter resulting from random composition fluctuations act as discrete emitters, but tunneling between emitters has significant impacts on the PL spectrum. It may be possible to exploit the mechanisms of Al and Ga segregation to form self-assembled QDs with more uniform structure and emission characteristics. This in turn will require a better fundamental understanding of the drivers of alloy fluctuations and cluster formation in nonplanar geometries,[29] which is an important area of future studies.

METHODS

Nanowire cores were grown on Si(111) substrates *via* the vapor−liquid−solid mechanism using Ga droplets as catalysts. The growth temperature was 630 °C and the V/III flux ratio was 10.8 under a Ga flux rate of 0.025 nm/s. Subsequently, the nanowire shell was deposited at a lower temperature of 490 °C and a total V/III flux ratio of 7.8 using a significantly higher Ga flux rate (0.17 nm/s). This change of growth conditions resulted in crystallization of the Ga catalyst and further promoted vapor−solid deposition at the {110} sidewall surfaces. The Al flux was selected to obtain an AlGaAs shell composition with a nominal Al mole fraction of 30%. Planar reference samples with 100 nm AlGaAs thickness were grown under identical conditions as the nanowires, *i.e.*, using the same V/III ratio, Ga flux rate and growth temperature. These planar films were grown on nonpolar (110) GaAs substrates to mimic exactly the same growth orientation and growth kinetics as the AlGaAs shell deposited at the {110} radial sidewall surfaces.

The PL measurements were carried out at 10 K and a semiconductor laser diode emitting at 532 nm was used for optical excitation. The laser was focused to a diffraction limited spot of ~1 μm in diameter onto the sample with an objective mounted to a closed loop piezo stage for fine position control. The PL was collected through the same objective and analyzed in a Princeton Instruments Acton spectrometer equipped with a liquid N_2 cooled multichannel CCD detector.

To prepare samples for atom probe tomography (APT), nanowires were transferred from the growth substrate to a half-cut TEM Cu mesh grid. A nanowire attached to the TEM grid was picked up and attached to a tungsten probe tip by a nanomanipulator in vacuum. Platinum deposition induced by an electron beam was performed to weld the nanowire to the probe tip. The probe tip was then transferred directly into the atom probe.

The nextnano[3] software was used to solve the 3D Schrödinger equation for the elliptical clusters presented in the manuscript. The single band effective mass approximation is used to find the energy eigenvalues and wave functions for heavy holes and electrons. The attractive Coulomb interaction between electron and hole (single neutral exciton) is also taken into account. In order to determine the exciton energy, the Schrödinger equation for electrons is solved: $(H + V_h)\Psi_e = E'_e\Psi_e$, and similarly for holes: $(H + V_e)\Psi_h = E'_h\Psi_h$. Here, H is the Hamiltonian without the Coulomb interaction (single particle approximation), $\Psi_{e/h}$ is the wave function, $E'_{e/h}$ is the resulting energy eigenvalue and $V_{e/h}$ is the electrostatic potential as determined by the Poisson equation from electron/hole wave function. The system of equations is solved iteratively by nextnano[3] until a self-consistent solution of the Schrödinger and Poisson equation is found. The exciton energy, *i.e.*, the transition energy, is then given as $E_X = E'_e - E'_h + 1/2 \times (\langle\Psi_h|V_e|\Psi_h\rangle - \langle\Psi_e|V_h|\Psi_e\rangle)$, where the matrix elements $\langle\Psi_h|V_e|\Psi_h\rangle$ and $\langle\Psi_e|V_h|\Psi_e\rangle$ are energy corrections to compensate for the fact that the attractive Coulomb energy was included twice, both for the electron and hole. More details about the simulation of excitonic effects can be found in the official nextnano[3] documentation.

Conflict of Interest: The authors declare no competing financial interest.

Acknowledgment. L.J.L. and N.J. acknowledge NSF DMR-1308654 for support of this work. We gratefully acknowledge financial support from the German Science Foundation (DFG) *via* SFB 631 and the Emmy Noether Program (HJK, KR3790/2-1), the Nanosystems Initiative Munich and the TUM-IAS Focus group "Nanophotonics". We acknowledge Stefan Birner for support and advice regarding the nextnano3 simulation software. This work was also supported by the EU FP 7 project SOLID, the German

Academic Exchange Service (DAAD), and the TUM International Graduate School for Science and Engineering (IGSSE). Atom-probe tomography was performed at the Northwestern University Center for Atom-Probe Tomography (NUCAPT). NUCAPT is a Shared Facility at the Materials Research Center of Northwestern University, supported by the National Science Foundation's MRSEC program (DMR-1121262).

Supporting Information Available: The Supporting Information is available free of charge on the ACS Publications website at DOI: 10.1021/acsnano.5b04070.

Peak fittings of photoluminescence spectrum; extended analysis of atom probe tomography including spatial distribution map, comparisons of Ga mole fraction maps and total hit density maps, cluster size distributions at different grid settings, and composition analysis of GaAs-AlGaAs planar reference samples; electron probability distributions for two neighboring clusters. (PDF)

REFERENCES AND NOTES

1. Yoon, J.; Jo, S.; Chun, I. S.; Jung, I.; Kim, H.-S.; Meitl, M.; Menard, E.; Li, X.; Coleman, J. J.; Paik, U.; *et al.* GaAs photovoltaics and optoelectronics using releasable multilayer epitaxial assemblies. *Nature* **2010**, *465*, 329–333.
2. Noborisaka, J.; Motohisa, J.; Hara, S.; Fukui, T. Fabrication and characterization of freestanding GaAs/AlGaAs core-shell nanowires and AlGaAs nanotubes by using selective-area metalorganic vapor phase epitaxy. *Appl. Phys. Lett.* **2005**, *87*, 093109.
3. Tambe, M. J.; Lim, S. K.; Smith, M. J.; Allard, L. F.; GradeCak, S. Realization of defect-free epitaxial core-shell GaAs/AlGaAs nanowire heterostructures. *Appl. Phys. Lett.* **2008**, *93*, 151917.
4. Morkötter, S.; Jeon, N.; Rudolph, D.; Loitsch, B.; Spirkoska, D.; Hoffmann, E.; Döblinger, M.; Matich, S.; Finley, J. J.; Lauhon, L. J.; *et al.* Demonstration of Confined Electron Gas and Steep-Slope Behavior in Delta-Doped GaAs-AlGaAs Core−Shell Nanowire Transistors. *Nano Lett.* **2015**, *15*, 3295–3302.
5. Mayer, B.; Rudolph, D.; Schnell, J.; Morkötter, S.; Winnerl, J.; Treu, J.; Müller, K.; Bracher, G.; Abstreiter, G.; Koblmüller, G.; *et al.* Lasing from individual GaAs-AlGaAs core-shell nanowires up to room temperature. *Nat. Commun.* **2013**, *4*, 2931.
6. Ho, J.; Tatebayashi, J.; Sergent, S.; Fong, C. F.; Iwamoto, S.; Arakawa, Y. Low-Threshold near-Infrared GaAs−AlGaAs Core−Shell Nanowire Plasmon Laser. *ACS Photonics* **2015**, *2*, 165–171.
7. Tomioka, K.; Motohisa, J.; Hara, S.; Hiruma, K.; Fukui, T. GaAs/AlGaAs Core Multishell Nanowire-Based Light-Emitting Diodes on Si. *Nano Lett.* **2010**, *10*, 1639–1644.
8. Chuang, L. C.; Sedgwick, F. G.; Chen, R.; Ko, W. S.; Moewe, M.; Ng, K. W.; Tran, T.-T. D.; Chang-Hasnain, C. GaAs-Based Nanoneedle Light Emitting Diode and Avalanche Photodiode Monolithically Integrated on a Silicon Substrate. *Nano Lett.* **2011**, *11*, 385–390.
9. Rudolph, D.; Funk, S.; Döblinger, M.; Morkötter, S.; Hertenberger, S.; Schweickert, L.; Becker, J.; Matich, S.; Bichler, M.; Spirkoska, D.; *et al.* Spontaneous Alloy Composition Ordering in GaAs-AlGaAs Core−Shell Nanowires. *Nano Lett.* **2013**, *13*, 1522–1527.
10. Heiss, M.; Fontana, Y.; Gustafsson, A.; Wust, G.; Magen, C.; O'Regan, D. D.; Luo, J. W.; Ketterer, B.; Conesa-Boj, S.; Kuhlmann, A. V.; *et al.* Self-assembled quantum dots in a nanowire system for quantum photonics. *Nat. Mater.* **2013**, *12*, 439–444.
11. Mancini, L.; Fontana, Y.; Conesa-Boj, S.; Blum, I.; Vurpillot, F.; Francaviglia, L.; Russo-Averchi, E.; Heiss, M.; Arbiol, J.; Morral, A. F. i.; *et al.* Three-dimensional nanoscale study of Al segregation and quantum dot formation in GaAs/AlGaAs core-shell nanowires. *Appl. Phys. Lett.* **2014**, *105*, 243106.
12. Weiß, M.; Kinzel, J. B.; Schülein, F. J. R.; Heigl, M.; Rudolph, D.; Morkötter, S.; Döblinger, M.; Bichler, M.; Abstreiter, G.; Finley, J. J.; *et al.* Dynamic Acoustic Control of Individual Optically Active Quantum Dot-like Emission Centers in Heterostructure Nanowires. *Nano Lett.* **2014**, *14*, 2256–2264.
13. Weiß, M.; Schülein, F. J. R.; Kinzel, J. B.; Heigl, M.; Rudolph, D.; Bichler, M.; Abstreiter, G.; Finley, J. J.; Wixforth, A.; Koblmüller, G.; *et al.* Radio frequency occupancy state control of a single nanowire quantum dot. *J. Phys. D: Appl. Phys.* **2014**, *47*, 394011.
14. Shi, T.; Jackson, H. E.; Smith, L. M.; Jiang, N.; Gao, Q.; Tan, H. H.; Jagadish, C.; Zheng, C.; Etheridge, J. Emergence of Localized States in Narrow GaAs/AlGaAs Nanowire Quantum Well Tubes. *Nano Lett.* **2015**, *15*, 1876–1882.
15. Chen, G.; Sun, G.; Ding, Y. J.; Prete, P.; Miccoli, I.; Lovergine, N.; Shtrikman, H.; Kung, P.; Livneh, T.; Spanier, J. E. Direct Measurement of Band Edge Discontinuity in Individual Core−Shell Nanowires by Photocurrent Spectroscopy. *Nano Lett.* **2013**, *13*, 4152–4157.
16. Versteegh, M. A. M.; Reimer, M. E.; Jöns, K. D.; Dalacu, D.; Poole, P. J.; Gulinatti, A.; Giudice, A.; Zwiller, V. Observation of strongly entangled photon pairs from a nanowire quantum dot. *Nat. Commun.* **2014**, *5*, 5298.
17. Borgström, M. T.; Zwiller, V.; Müller, E.; Imamoglu, A. Optically Bright Quantum Dots in Single Nanowires. *Nano Lett.* **2005**, *5*, 1439–1443.
18. Bulgarini, G.; Reimer, M. E.; Bouwes Bavinck, M.; Jöns, K. D.; Dalacu, D.; Poole, P. J.; Bakkers, E. P. A. M.; Zwiller, V. Nanowire Waveguides Launching Single Photons in a Gaussian Mode for Ideal Fiber Coupling. *Nano Lett.* **2014**, *14*, 4102–4106.
19. Riley, J. R.; Padalkar, S.; Li, Q.; Lu, P.; Koleske, D. D.; Wierer, J. J.; Wang, G. T.; Lauhon, L. J. Three-Dimensional Mapping of Quantum Wells in a GaN/InGaN Core−Shell Nanowire Light-Emitting Diode Array. *Nano Lett.* **2013**, *13*, 4317–4325.
20. Rigutti, L.; Blum, I.; Shinde, D.; Hernández-Maldonado, D.; Lefebvre, W.; Houard, J.; Vurpillot, F.; Vella, A.; Tchernycheva, M.; Durand, C.; *et al.* Correlation of Microphotoluminescence Spectroscopy, Scanning Transmission Electron Microscopy, and Atom Probe Tomography on a Single Nano-object Containing an InGaN/GaN Multiquantum Well System. *Nano Lett.* **2014**, *14*, 107–114.
21. Benallali, H.; Cremel, T.; Hoummada, K.; Mangelinck, D.; André, R.; Tatarenko, S.; Kheng, K. Atomic scale investigations on $Cd_xZn_{1-x}Se$ quantum dots: Correlation between the composition and emission properties. *Appl. Phys. Lett.* **2014**, *105*, 053103.
22. Martin, A. J.; Hunter, A. H.; Saucer, T. W.; Sih, V.; Marquis, E. A.; Millunchick, J. Atom probe tomography analysis of different modes of Sb intermixing in GaSb quantum dots and wells. *Appl. Phys. Lett.* **2013**, *103*, 122102.
23. Birner, S.; Zibold, T.; Andlauer, T.; Kubis, T.; Sabathil, M.; Trellakis, A.; Vogl, P. nextnano: General Purpose 3-D Simulations. *IEEE Trans. Electron Devices* **2007**, *54*, 2137–2142.
24. Ramsteiner, M.; Hey, R.; Klann, R.; Jahn, U.; Gorbunova, I.; Ploog, K. H. Influence of composition fluctuations in Al(Ga)As barriers on the exciton localization in thin GaAs quantum wells. *Phys. Rev. B: Condens. Matter Mater. Phys.* **1997**, *55*, 5239–5242.
25. Hsieh, K. C.; Hsieh, K. Y.; Hwang, Y. L.; Zhang, T.; Kolbas, R. M. Strain-induced phase separation in annealed low-temperature grown $Al_{0.3}Ga_{0.7}As$. *Appl. Phys. Lett.* **1996**, *68*, 1790–1792.
26. Johnson, M. B.; Maier, U.; Meier, H. P.; Salemink, H. W. M. Atomic-scale view of AlGaAs/GaAs heterostructures with cross-sectional scanning tunneling microscopy. *Appl. Phys. Lett.* **1993**, *63*, 1273–1275.
27. Salemink, H.; Albrektsen, O. Atomic-scale composition fluctuations in III-V semiconductor alloys. *Phys. Rev. B: Condens. Matter Mater. Phys.* **1993**, *47*, 16044–16047.
28. Petroff, P.; Cho, A.; Reinhart, F.; Gossard, A.; Wiegmann, W. Alloy Clustering in $Ga_{1-x}Al_xA$ Compound Semiconductors Grown by Molecular Beam Epitaxy. *Phys. Rev. Lett.* **1982**, *48*, 170–173.

29. Zheng, C.; Wong-Leung, J.; Gao, Q.; Tan, H. H.; Jagadish, C.; Etheridge, J. Polarity-Driven 3-Fold Symmetry of GaAs/AlGaAs Core Multishell Nanowires. *Nano Lett.* **2013**, *13*, 3742–3748.
30. Schedelbeck, G.; Wegscheider, W.; Bichler, M.; Abstreiter, G. Coupled Quantum Dots Fabricated by Cleaved Edge Overgrowth: From Artificial Atoms to Molecules. *Science* **1997**, *278*, 1792–1795.
31. Krenner, H. J.; Sabathil, M.; Clark, E. C.; Kress, A.; Schuh, D.; Bichler, M.; Abstreiter, G.; Finley, J. J. Direct Observation of Controlled Coupling in an Individual Quantum Dot Molecule. *Phys. Rev. Lett.* **2005**, *94*, 057402.
32. Stinaff, E. A.; Scheibner, M.; Bracker, A. S.; Ponomarev, I. V.; Korenev, V. L.; Ware, M. E.; Doty, M. F.; Reinecke, T. L.; Gammon, D. Optical Signatures of Coupled Quantum Dots. *Science* **2006**, *311*, 636–639.
33. Müller, K.; Bechtold, A.; Ruppert, C.; Zecherle, M.; Reithmaier, G.; Bichler, M.; Krenner, H. J.; Abstreiter, G.; Holleitner, A. W.; Villas-Boas, J. M.; *et al.* Electrical Control of Interdot Electron Tunneling in a Double InGaAs Quantum-Dot Nanostructure. *Phys. Rev. Lett.* **2012**, *108*, 197402.
34. Ortner, G.; Bayer, M.; Larionov, A.; Timofeev, V. B.; Forchel, A.; Lyanda-Geller, Y. B.; Reinecke, T. L.; Hawrylak, P.; Fafard, S.; Wasilewski, Z. Fine Structure of Excitons in InAs/GaAs Coupled Quantum Dots: A Sensitive Test of Electronic Coupling. *Phys. Rev. Lett.* **2003**, *90*, 086404.